equation has one real root and two complex roots. When (54) becomes an equality two of the three real roots are real. Locating the roots on the x plane allows one to define the branch cuts as shown on Fig. 5. It is of interest to discuss the discontinuous behavior of ψ at the edge of the sheet i.e., at $\zeta = 0$. Actually $\zeta \to 0$ at $x \to 1$. Since the path of integration is on the real axis of x, it is evident that ψ is discontinuous near $x = 1$ for $x_3 < 1$. But the position of the roots on the x plane follow the directions of the arrows as indicated on Fig. 5, when a, b acquire different values. When x_3 tends to unit, $x = 1$ is no longer a branch point and ψ is continuous in the vicinity of $x = 1$. It is readily checked by means of (51) that the necessary condition for this to happen is $b = 1$.

The dependence of the potential ψ on the coordinate ζ is shown in graphical form in Fig. 6.

ACKNOWLEDGMENTS

This work was supported in part by the National Aeronautics and Space Administration and Cambridge Air Force Research Center and in part by the Lawrence Radiation Laboratory, University of California, Livermore where the author spent part of the summer.

THE PHYSICS OF FLUIDS SUPPLEMENT 1964

Current Speed in a Magnetic Annular Shock Tube

JAMES KECK
Avco-Everett Research Laboratory, Everett, Massachusetts

A parametric study of the speeds of the current sheet and center-of-gravity of current in a magnetic annular shock tube has been carried out. The parameters varied include: (1) the drive current, (2) the polarity of the inner electrode, (3) the gas pressure, (4) the nature of the gas, (5) the radius of the inner electrode and (6) the material of the inner electrode. The most interesting result of the investigation was the observation of limiting speeds for the current sheet and center-of-gravity of current of approximately 8 cm/μsec and 3 cm/μsec, respectively. These speeds were not exceeded even under conditions where the magnetic pressure exceeded the dynamic pressure by a factor of 10. The most probable explanation of the limiting speed is that it is due to the inertial drag of material ablated from the insulator at the driver end of the shock tube.

INTRODUCTION

IN a magnetic annular accelerator, gas in the space between two coaxial electrodes is accelerated by the magnetic pressure behind a current sheet maintained between the electrodes by a condenser discharge. Such accelerators have potential applications as engines for space propulsion, plasma injectors for fusion devices, and shock tubes for the study of gas dynamics in the speed range beyond that which can be reached by thermal or chemical means. Where the interest is in shock tube applications, the device has been called a "magnetic annular shock tube"[1] and the gas is introduced at a uniform pressure; where the interest is in propulsion or plasma injection, the accelerator is often called a "plasma gun"[2] and the gas is introduced as a puff. Although considerable study has been devoted to both modes of operation, neither practical applications nor a satisfactory theory of the operation of such accelerators have yet been achieved.

The present investigation represents an attempt to obtain a better understanding of the factors effecting the speed of the current sheet in a magnetic annular shock tube having a large radius ratio and no externally applied bias fields. It was motivated by evidence obtained in a previous investigation[3] of the shape of the current sheet that serious discrepancies between the measured and predicted[4,5] sheet speeds were occurring. Since the sheet speed is one of the most important and, in principle, easiest parameters to predict, this was considered quite serious. In this connection it should be noted that in a similar shock tube having a small radius ratio and magnetic bias fields, Patrick[1] has produced

[1] R. M. Patrick, Phys. Fluids **2**, 589 (1959).
[2] J. Marshall, Phys. Fluids **3**, 135 (1960).
[3] J. C. Keck, Phys. Fluids **5**, 630 (1962).
[4] N. H. Kemp and H. E. Petschek, Phys. Fluids **2**, 599 (1959).
[5] P. M. Mostov, J. L. Neuringer, and D. S. Rigney, Phys. Fluids **4**, 1097 (1961).

magnetically driven shock waves which do move at the theoretical velocity. Although the origin of this apparent difference in operation is not fully understood, Fishman and Petschek[6,7] have shown that both the radius ratio and the bias fields have an important effect on the performance of a magnetic annular shock tube and that Patrick's shock tube may be expected to operate in a completely different manner than the one used in the present investigation. Thus to a large extent, Patrick's results must be regarded as applying to a different class of shock tubes, and there is no real contradiction between his results and those reported in this paper.

The usual approximation made in obtaining an expression for the sheet speed is to use the "slug model." This model assumes that all the gas swept up by the current sheet moves at the sheet speed and that wall friction may be neglected. Under these conditions the momentum equation becomes (mks units)

$$\frac{B^2}{2\mu_0} = \frac{du}{dt}\int_0^z \rho_1\, dz + \frac{\rho_1 u^2}{(1 - \rho_1/\rho_2)}, \qquad (1)$$

where B is the magnetic field immediately behind the current sheet, μ_0 is the vacuum permeability, u is the speed of the current sheet, z is the axial position of the front of the slug, and ρ_1 and ρ_2 are, respectively, the gas densities ahead of and in the slug. In order to obtain the density ratio ρ_1/ρ_2 one must employ the equations of mass and energy conservation and the equation of state. However, in most of the cases we shall consider ρ_1/ρ_2 is small enough so that it can be neglected compared to one without significant error.

Equation (1) provides a fundamental check on the operation of any magnetic accelerator. Failure of the measurements to fulfill this equation implies a basic difficulty in either the operation of the accelerator or the experimental techniques. Unfortunately, it is difficult to use this equation in the case of plasma guns,[2,8,9] where the gas is introduced in a puff, due to the uncertainty in the initial density distribution. Thus, if achieving an understanding of the acceleration mechanism is the goal of an experiment, operation of the accelerator as a shock tube at constant initial density is desirable. A number of such shock tube investigations[1,3,10-12] have been carried out and although some measure of agreement with Eq. (1) has been reported, the situation is far from satisfactory. Most of the measurements have been made in shock tubes having a radius ratio greater than 3 so that the magnetic pressure varies by more than a factor of 9 across the annulus and there exists considerable ambiguity about just how one should employ Eq. (1). Furthermore, it has been shown[3,12] that the sheet speed in a shock tube of typical design depends on the polarity of the inner electrode. Finally, in most cases the current pulse had the form of a damped sine wave so that the speed varied continuously and was, therefore, difficult to determine precisely. These considerations combined with the fact that the results of different investigators employing similar devices do not agree with the precision one would expect, have produced a confused situation which leaves one in considerable doubt as to what is occurring in such large radius ratio magnetic annular shock tubes.

In the present study we have concentrated on measurements of the speed of the current sheet and back electromagnetic force in the shock tube. To provide information which would give a reasonable check on the predictions of the momentum equation and provide an overlap with the work of other investigators, as many of the parameters effecting operation of the shock tube were varied as possible within the physical limitations of the experimental setup. These include: (1) the driving current, (2) the polarity of the inner electrode, (3) the gas pressure, (4) the nature of the gas, (5) the radius of the inner electrode, and (6) material of the inner electrode. The operation was also studied with the center electrode replaced by a button to simulate conditions encountered in "conical" shock tubes. The only parameters not varied were the radius of the outer electrode and the material of the insulators at the ends of the device. As we shall see in the discussion, failure to vary the material of the insulators deprived us of a valuable piece of information bearing on the interpretation of the results, but the shock tube was dismantled before this could be easily rectified.

The most significant result of the investigation was the observation of a "limiting speed" beyond which it was not possible to drive the current sheet

[6] F. Fishman and H. E. Petschek, Phys. Fluids **5**, 632 (1962).
[7] F. Fishman and H. E. Petschek, Phys. Fluids **5**, 1188 (1962).
[8] B. Forowitz and P. Gloersen, General Electric (Philadelphia), Report R60SD456 (1960).
[9] L. C. Burkhardt and R. H. Lovberg, Phys. Fluids **5**, 341 (1962).
[10] A. Dattner, in *Proceedings of the Fourth International Conference on Ionization Phenomena in Gases*, (North-Holland Publishing Company, Amsterdam, 1960), Vol. II, p. 1151.
[11] C. T. Chang, Phys. Fluids **4**, 1085 (1961).
[12] P. J. Hart, Phys. Fluids **5**, 38 (1962).

even under conditions where the total magnetic pressure exceeded the dynamic pressure by more than an order of magnitude. This "limiting speed" was substantially independent of any of the parameters which were varied in the experiment and provides clear evidence for an important source of drag on the current sheet in addition to that due to the dynamic pressure of the gas initially in the shock tube. Estimates of the effect of the boundary layer on the walls of the shock tube show that it is unlikely to be the result of wall friction. It is also unlikely to be associated with the drag due to positive ions striking the cathode in the case where the ions carry the current. The most plausible hypothesis is that it is associated with the inertia of material ablated from the insulator at the driving end of the shock tube. This material is ionized either by photons or electron impact and becomes entrained by the currents. A simplified theory of the process based on the assumption of a steady state ablating boundary layer on the insulating wall leads to a qualitatively correct description of the observations. To make the theory quantitative, one must calculate the thickness of the boundary layer. This is a problem beyond the scope of the present paper which involves (1) the heat of vaporization and vapor pressure law for the wall material, (2) the electrical and thermal conductivity of the ablation products, (3) cross-sections for ionization of ablation products by photons and electrons, (4) energy dissipation by ion slip and (5) photon production in the gas and at the electrodes. Nevertheless the problem does appear tractable and a full theory of such a boundary layer should have many important applications.

EXPERIMENTAL APPARATUS

A schematic diagram of the magnetic annular shock tube used in the experiments is shown in Fig. 1. It is identical with that used in the previous studies of shock shape[3] and consists of a cylindrical copper outer electrode 6 in. in diameter and 34 in., long and an interchangeable inner electrode. The insulators at the ends of the device were lucite sealed to the electrodes by ○ rings. The tube was pumped through a series of 8 slots arranged symmetrically around the outer electrode 2 in. from the driver end and could be evacuated to a pressure of a few tenths of a micron.

To preserve cylindrical symmetry, the shock tube was connected to the condenser bank through a 2 ft section of coaxial line terminating in a triggered spark gap. The measured inductance L_0 of this line was 0.06 μH. The condenser bank was connected to

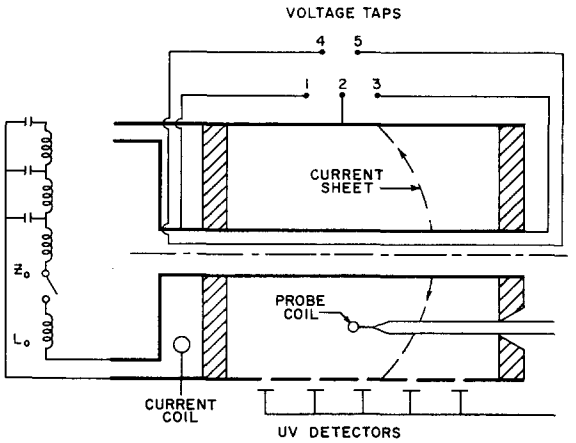

FIG. 1. Schematic diagram of magnetic annular shock tube.

form a lumped constant line having a total capacity C_0 of 384 μF and a characteristic impedance Z_0 of 0.023 Ω. The system operated reliably at positive or negative voltages V_0 between 2 and 10 kV and a produced current pulse which rose with a time constant of 1.5 μsec and was approximately constant for about 10 μsec when discharged through a matched load. Under most conditions the impedance of the shock tube was small compared to Z_0 and the steady value of the current was approximately V_0/Z_0.

To maintain reasonable gas purity a continuously operating flow system was used which changed the gas in the tube once a minute. The pressure was measured by an Alphatron gauge.

Provision for pre-ionizing the gas was provided by four small button electrodes symmetrically placed in the insulating wall at the driver end of the shock tube. These were individually connected to four 2 μF–10 kV condensers which could be discharged simultaneously through a single switch. Pre-ionization made no significant difference in the operation of the shock tube after breakdown, but it did eliminate delays in breakdown and was normally employed for this reason. It may be noted in this connection that no matter where the initial breakdown occurred in the tube, the main current sheet always originated at the driving end. The reason for this is that radiation from the initial streamer photoionizes the gas and makes it a sufficiently good conductor to prevent further penetration of the magnetic field.

The "optical speed" of the discharge was measured by a series of 5 tungsten photoelectric detectors of a type developed by Camac[13,14] spaced at 6 in. inter-

[13] M. Camac, A. Kantrowitz, M. Litvak, R. M. Patrick, and H. E. Petschek, Nucl. Fusion Suppl., Pt. 2, 423 (1962).
[14] R. M. Patrick and M. Camac, *Plasma Hydromagnetics* (Stanford University Press, Stanford, California, 1962), p. 97.

vals along the length of the tube. Tungsten detectors operating in UV were used in preference to photomultipliers operating in the visible because they gave cleaner signals, are extremely stable and are unaffected by scattered light. The light entering the tungsten detectors was collimated by two 1 mm holes spaced 2 cm apart giving a solid angle area product $\Omega A = 1.5 \times 10^{-5}$ cm^2 sr and a maximum spot diameter of 7.5 mm at the axis of the tube.

The current waveform was measured by a one turn rectangular coil feeding directly into a terminated 93 cable. Voltage wave forms were measured through 100 K attenuators connected to terminals at both ends of the center electrode as indicated in Fig. 1. An additional flux loop passing through the center electrode and around the test section was used as a check on V_{13}. As long as the driver currents do not penetrate to the outside of the electrodes the voltage from the flux loop V_{45} should be identical to V_{13}. This was always the case in the present experiments.

To study conditions in the interior of the shock tube scanning probes could be inserted through ○-ring seals in the outside electrode or the terminal wall as shown in Fig. 1.

EXPERIMENTAL MEASUREMENTS

Summary of Conditions

Measurements were made over a range of driver currents I_0 from 40 to 400 kA and initial pressures p_1 from 50 to 1000 μHg corresponding to initial particle densities n_1 from 1.8×10^{15} to 3.6×10^{16} cm^{-3}. The test gases employed were hydrogen, helium, air and argon. Copper center electrodes $\frac{1}{4}$, 1, 2, and 4 in. diameter and a stainless steel electrode of 2 in. diameter were used in the study. In addition, a short series of experiments was performed in which all but a short segment of the center electrode was omitted or replaced by Teflon or Pyrex rods.

In all cases the center electrode was run both positive and negative since previous experiments[3] had indicated that the shape and speed of the current sheet were polarity dependent. Although the present measurements also showed a polarity dependence the effects were relatively small, and we have in general given the results only for the negative case since this has been the most common mode of operation in other laboratories.

Current and Voltage Measurements

A typical set of current and voltage wave forms for both positive and negative center electrode is

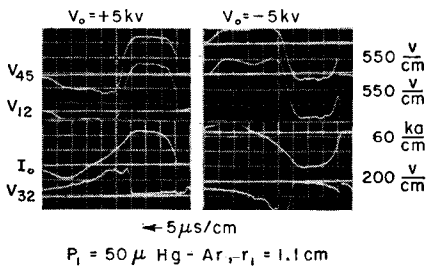

FIG. 2. Typical oscillograms showing the current and voltage waveforms for positive and negative operation of the magnetic annular shock tube. The voltage subscripts refer to the terminals shown in Fig. 1.

shown in Fig. 2. The traces from top to bottom are the flux loop voltage V_{45}, the driving voltage V_{12}, the driver current I_0 and the terminal voltage V_{32}. Reasonably steady conditions are obtained for a test time of 10 to 15 μsec and except for the polarity of the signals, there is relatively little difference between positive and negative operation. It is interesting to note that while V_{45} and V_{12} both exceed 1200 V during the test time, V_{32} remains less than 50 V until the current interface strikes the terminal insulator at which time it rises abruptly to a value of over 300 V. This shows that only a small fraction of the total power supplied to the device is being dissipated by the arc drop and that the gas ahead of the current sheet is a sufficiently good conductor to prevent any appreciably diffusion of current to the terminal wall. It is also interesting to note that while V_{45}, V_{12} and I_0 oscillate as a result of the impedance mismatch between the shock tube and the current source, V_{32} never changes sign. Since V_{32} has the sign of the current at the terminal end, this shows that current loops are being formed within the shock tube each time the driver current changes sign.

An important parameter which may be obtained from the type of data shown in Fig. 2 is the flux speed u_L. The flux speed is the axial speed of the center-of-gravity of the current density in the shock tube and is defined by the equation

$$u_L = \frac{1}{L' I_0}\left(\frac{d\phi}{dt} - \frac{\phi}{I_0}\frac{dI_0}{dt}\right), \tag{2}$$

where $d\phi/dt = V_{45}$ is the rate of change of magnetic flux through the flux loop, $L' = (\mu_0/2\pi)\ln(r_2/r_1)$ is the inductance per unit length of the shock and (r_2/r_1) is radius ratio for the electrodes. During the steady test time, the term involving dI/dt may be neglected and

$$u_L \approx E_{45}/B_0, \tag{3}$$

where $E_{45} = V_{45}/r\ln(r_2/r_1)$ and $B_0 = \mu_0 I_0/2\pi r$. It

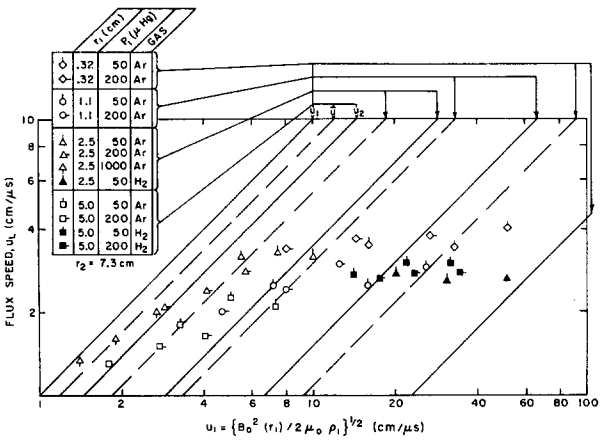

FIG. 3. Flux speed u_L as a function of the parametric speed u_1 for a variety of shock tube operating conditions. The diagonal lines show the values of the parametric speeds u_2 and $\bar{u}$ defined by Eqs. (5) and (6) for each value of the inner electrode radius. The data shown were obtained with a negative center electrode; speeds obtained with a positive electrode were the same within ±10%.

should be noted that E_{45}/B_0 is not the E/B velocity at the driver end except when the terminal voltage V_{23} is identically zero and that measurement of the driving voltage V_{12} alone is insufficient to determine whether there is any axial motion of the current in a coaxial accelerator.

A plot of u_L as a function of the parametric speed

$$u_1 = [B_0^2(r_1)/2\mu_0\rho_1]^{\frac{1}{2}} \tag{4}$$

is shown in Fig. 3 for a variety of operating conditions. Note that u_1 is the speed obtained from Eq. (1) by balancing dynamic and magnetic pressures at the inside electrode and neglecting the term ρ_1/ρ_2. Also shown in Fig. 3 by the diagonal lines are the parametric speeds

$$u_2 = [B_0^2(r_2)/2\mu_0\rho_1]^{\frac{1}{2}} \tag{5}$$

obtained by balancing dynamic and magnetic pressures at the outside electrode, and

$$\bar{u} = [\tfrac{1}{2}L'I_0^2/\pi(r_2^2 - r_1^2)\rho_1]^{\frac{1}{2}} \tag{6}$$

obtained by balancing the integrated dynamic and magnetic pressures. When plotted as a function of u_1 all of the data fall more or less on a common curve which is asymptotic to u_1 for small values of u_1 but levels off at a value of 3 cm/μsec for large values of u_1. When plotted as a function of either u_2 or $\bar{u}$ no simple correlation is evident and the data scatter widely. This shows that for high values of u_1 Eq. (1) is not valid and there must exist an important drag on the current in the shock tube in addition to the inertial drag of the test gas.

A second parameter which may be obtained from the type of data shown in Fig. 2 is the value of terminal voltage V_{32}. Typical values of V_{32} during the steady test time are shown in Fig. 4 as a function of the current per unit circumference of the inner electrode $I_0/2\pi r_1$. This gave the best simple correlation of the data that could be found. It can be seen that V_{32} is roughly inversely proportional to $I_0/2\pi r_1$. If we assume that V_{32} is related to the arc drop at the center electrode and that the arc spot has a length of about 10 cm as indicated by data to be presented later, this leads to an approximately constant power dissipation in the boundary layer at the inner electrode of 40 kW/cm^2. If this power goes into the copper it will only raise the surface temperature of the wall of the order of 10°K which is insignificant. However, if it goes into ablation of a surface layer of impurities, as it probably does, it is sufficient to produce a particle flux of the order of 10^{23} sec^{-1} cm^{-2} which is comparable to the particle flux incident on the current sheet and could have a significant effect on the flow near the electrodes.

Ultraviolet Light Measurements

A typical set of oscillograms obtained using the tungsten UV photoelectric detectors is shown in Fig. 5 for discharges in H_2, He, air, and Ar all at the same pressure and driving voltage. The lower traces show the outputs of the five UV detectors feeding into a terminated 93Ω cable and the upper traces show

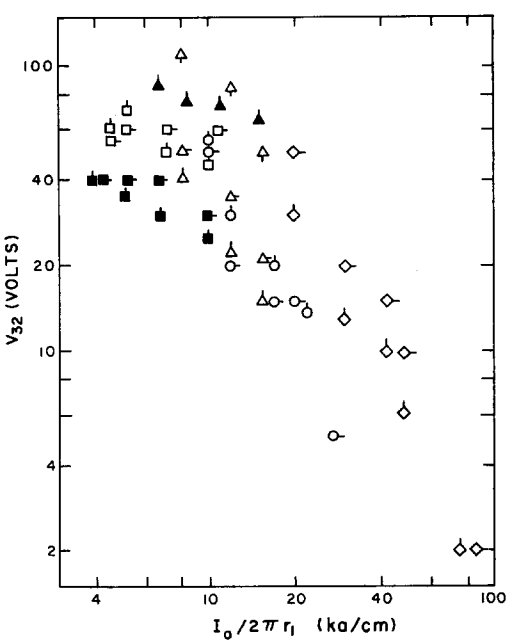

FIG. 4. Terminal voltages V_{32} as a function of current per unit circumference of the inner electrode $I_0/2\pi r_1$. The points are coded as in Fig. 3. The voltages are for negative operation; voltages for positive operation were similar.

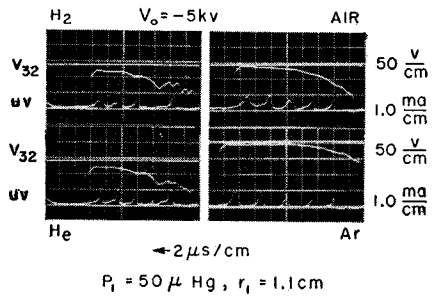

FIG. 5. Representative oscillograms showing the output of the 5 tungsten UV detectors (lower traces) along with the terminal voltage V_{32} (upper traces) for discharges in H_2, He, air, and Ar all under the same conditions.

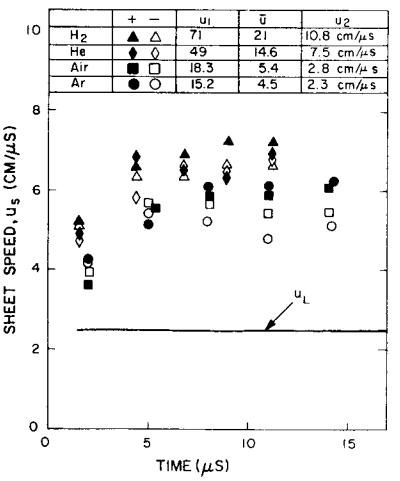

FIG. 6. Speed u_s of current sheet as a function of time for conditions corresponding to those of Fig. 5. Data for both positive and negative center electrode are shown. Also shown is the flux speed u_L deduced from the flux loop voltage using Eq. (2) and the parametric speeds u_1, u_2 and $\bar{u}$ defined by Eqs. (4)–(6).

the terminal voltage V_{32} which gives an indication of the arrival time of the current sheet at the end wall of the shock tube 4 in. beyond the last detector. By inserting probes through the terminal wall of the shock tube to shadow the UV detectors, it has been established that most of the light observed comes from the arc spot on the inside electrode. It has further been established that the position of this spot correlates exactly with the position of the leading current sheet in the shock tube and that no significant shock wave precedes it.[3] Thus, the records in Fig. 5 give the speed of the leading current sheet down the shock tube. It can be seen that, except for the first interval during which the current is rising, the sheet speed is essentially constant over the entire length of the shock tube. It can also be seen that this speed is very nearly independent of the molecular weight of the gas, which again indicates that the major drag on the current is not due to the inertia of the test gas. According to Eq. (1), a current sheet propagating in H_2 at uniform speed should move at 4.5 time the speed of a sheet propagating in Ar when driven by the same magnetic pressure. This is clearly not the case and the observed speed in H_2 is only about 20% higher than that in Ar.

A somewhat more quantitative picture of the situation is given in Fig. 6 which shows the measured sheet speeds u_s plotted as a function of time for both positive and negative center electrodes. In addition to the features just discussed, the data in Fig. 6 confirms previously reported results that there is a polarity asymmetry with respect to u_s in which the sheet tends to propagate slightly faster when the center electrode is positive.

Also shown in Fig. 6 is the flux speed u_L deduced from the flux loop voltage V_{45}. Within the accuracy of measurement this was the same in all cases and only a single curve is shown. Note that u_L was constant over the entire range for which it could be determined even though I_0 and V_{45} were constant only in the interval from 5 to 15 μsec. It can be seen that u_L is less than half as large as u_s which indicates that the center-of-gravity of the current density is lagging considerably behind the position of the leading current sheet. This suggests that estimates of the specific impulse of a coaxial accelerator based on measurements of u_s may be seriously in error, since it is more reasonable to associate the speed of the bulk of the material with u_L than u_s.

A plot of the sheet speed u_s as a function of the parametric speed u_1 is shown in Fig. 7 for conditions corresponding to those of Fig. 3. It can be seen that u_s exhibits the same general trend as the flux speed u_L except that the correlation with u_1 is not quite as good and the limiting velocity is not quite so well defined since u_s is still rising slowly at the highest values of u_1 investigated.

In addition to the speed of the current sheet, we

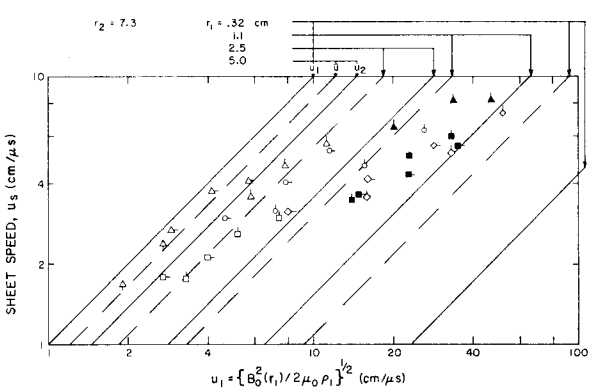

FIG. 7. Current sheet speed u_s as a function of the parametric speed u_1 for the same conditions as the data in Fig. 3. The points are coded as in Fig. 3. The speeds shown are for negative center electrode; the speeds for a positive center electrode are 10 to 20% higher.

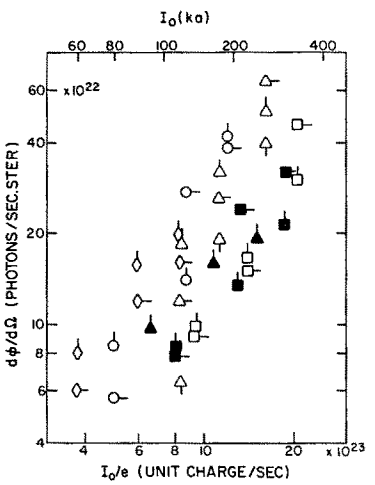

FIG. 8. Intensity of photons with energies above the tungsten photoelectric threshold (10 eV) coming from the arc spot on the inside electrode plotted as a function of the number of unit charges striking the electrode. The points are coded as in Fig. 3. The intensities shown are for a negative center electrode; the intensities for a positive center electrode were the same within the experimental scatter.

may also obtain an estimate of the intensity of UV radiation in the shock tube from photoelectric records of the type shown in Fig. 5. The photoelectric current I_p in the tungsten detectors is related to the spectral intensity $(d\phi/d\Omega)A\ d\nu$ of the incident UV radiation by the expression:

$$I_p = e\Omega A \int \epsilon_\nu (d\phi/d\Omega\ dA\ d\nu)\ d\nu, \qquad (7)$$

where e is the electronic charge, ΩA is the solid angle area product for the collimating holes and ϵ_ν is the quantum efficiency of the tungsten cathode. Data on the photoelectric efficiency of untreated tungsten summarized by Weissler[15] shows that ϵ_ν rises sharply from a threshold at $h\nu \approx 10$ eV to an approximately constant value of 0.1. Thus to a first approximation we may write

$$I_p = 0.1e\Omega A(d\phi/d\Omega\ dA), \qquad (8)$$

where $d\phi/d\Omega\ dA$ is the flux of photons per unit area per unit solid angle with energies above 10 eV falling on the detector. Since it is known that most of the photons entering the detector come from the arc spot on the inside electrode, we may obtain the total intensity per unit solid angle $d\phi/d\Omega$ normal to the electrode by integrating the output of the photo detectors with respect to time and multiply the result by $2\pi r_1 u_s$. This leads to the expression

$$\frac{d\phi}{d\Omega} = \frac{20\pi r_1 u_s}{e\Omega A} \int I_p\ dt. \qquad (9)$$

A plot of $d\phi/d\Omega$ as a function of the driving current I_0 is shown in Fig. 8. As can be seen in Fig. 5, signals from the UV detectors fluctuated considerably and the reproducibility of the measurements was about a factor of 3. Nevertheless, the order of magnitude of $d\phi/d\Omega$ is certainly correct and shows that if the angular distribution is isotropic, there is roughly one photon with energy in excess of 10 eV emitted for every unit charge that strikes the wall. It can also be seen that for any given inner electrode radius the intensity was roughly proportional to the driving current and independent of pressure or nature of the gas and the polarity of the center electrode. There does appear to be a tendency for the intensity to decrease as the electrode radius increases, but it is relatively weak and could easily be associated with a systematic error in the integration of the detector signals.

It is interesting to note that the photon intensity indicated is the right order of magnitude to provide sufficient photoelectric emission from the cathode to carry the primary current. It is also sufficient to produce substantial ionization of the gas ahead of the current sheet and we may reasonably expect this gas to have at least the room temperature conductivity of a fully ionized gas.[16]

Performance Without Center Electrode

The effect of omitting the conducting center electrode on the current, voltage, and speed characteristics of the shock tube is shown in Fig. 9. The records on the left were obtained using a brass button electrode 2.2 cm in diameter and 1 cm long connected to a $\frac{1}{4}$-in. copper rod running the remaining length of the shock tube; the records on the right were obtained using the same button electrode with the copper rod replaced by a 30 mil insulated wire

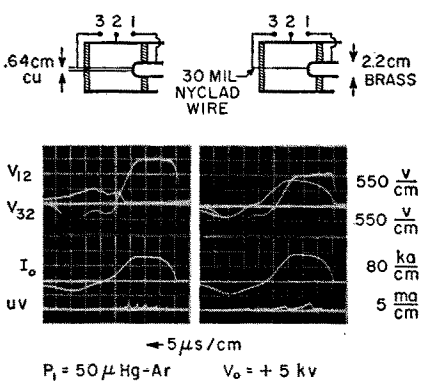

FIG. 9. Oscillograms showing current, voltage and speed histories for a magnetic annular shock tube with a conducting center electrode (right) and without a conducting center electrode (left). The records shown are for a positive center electrode; operation with a negative center electrode was substantially the same.

[15] G. L. Weissler, in *Handbuch der Physik*, edited by S. Flügge (Julius Springer-Verlag, Berlin, 1956), Vol. XXI, p. 342.

[16] L. Spitzer, *Physics of Fully Ionized Gases* (Interscience Publishers, Inc., New York, 1956).

for the purpose of making a voltage connection. By comparing the records of the driving voltage V_{12} and current I_0, it can be seen that the power input to the shock tube was nearly the same with or without a center electrode although the impedance was somewhat higher in the former case. However, the fraction of the power input which goes into magnetic acceleration of the gas is very different in the two cases. When the center electrode is present, the voltage $V_{13} = V_{12} - V_{32}$ associated with expansion of the current loop is over 97% of V_{12} during the entire test time; when the center electrode is absent V_{13} falls rapidly to less than 25% of V_{12} while V_{32} rises in a complementary manner. This indicates that when the center electrode is omitted the shock tube becomes primarily a heater and there is little expansion of the current loop.

A substantial decrease in the speed of the current sheet also occurs when the center electrode is omitted. This can be seen from the UV speed records in Fig. 9 and the plots in Fig. 10 of the sheet speed u_s and the flux speed u_L as functions of time. For purposes of this comparison, the effective diameter of the axial current used in Eq. (2) to compute u_L when the center electrode was absent was taken equal to $\frac{1}{4}$-in. Since the dependence of u_L on this diameter is only logarithmic, the results would not be altered much by assuming any other reasonable value and, in any case, the important qualitative result that the expansion of the current loop is small and diminishes rapidly is not effected.

The operation of the shock tube was also studied under conditions where all but the first few inches of the center electrode was insulated or replaced by Teflon or Pyrex rods, and was found to be substantially the same as when the center electrode was omitted.

Although the operating characteristics of shock tubes without center electrodes are of somewhat peripheral interest as far as the present paper is concerned, we have included this discussion to show the importance of a conducting center electrode in obtaining magnetic drive and because of the similarity between this geometry and that of the "conical" shock tubes.[17-21]

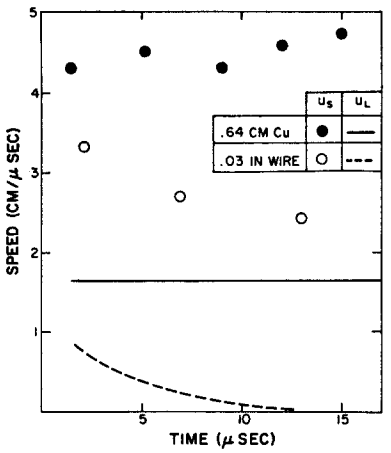

FIG. 10. Sheet speeds u_s and flux speeds u_L calculated from the data shown in Fig. 9.

DISCUSSION OF RESULTS

It appears from the results reported above that, under a wide variety of operating conditions, only a small fraction of the total drag in the magnetic annular shock tube is due to the inertia of the test gas. In this section we shall explore other possible sources of drag to see if we can obtain even a qualitative understanding of the results. The sources considered are: (1) drag due to the flow of ion current, (2) drag associated with boundary layer growth on the electrodes and (3) drag due to the ablation of material from the insulator at the driver end of the shock tube.

Ion Current Drag

It has been pointed out by Thom, Norwood, and Jaluka[22] that if the ions carry an appreciable fraction f of the current in a magnetic accelerator, there will be a drag associated with these ions striking the cathode. To calculate this drag we note that each ion carries with it an axial component of momentum mu_s and that the number of ions striking the cathode per second is fI_0/e. The product of these factors is the total drag due ion current and can be equated to the total magnetic pressure to obtain an expression for u_s. The result is

$$u_s = \frac{1}{2f}\left(\frac{e}{m}\right)L'I. \tag{10}$$

Although it is obvious that Eq. (10) does not predict a limiting speed and thus cannot provide the explanation we are seeking, it is interesting to compare the magnitude of the predicted speeds with those actually observed. Taking as an example the conditions corresponding to the data of Figs. 5 and 6 and

[17] V. Josephson, J. Appl. Phys. **29**, 30 (1958).
[18] V. S. Komelkov, Y. V. Skvortsov, S. S. Tserevitinov, and V. I. Vasiliev, in *Proceedings of the Fourth International Conference on Ionization Phenomena in Gases* (North-Holland Publishing Company, Amsterdam, 1960), Vol. II, p. 1141.
[19] F. R. Scott and R. F. Wenzel, Phys. Fluids **2**, 609 (1959).
[20] V. Josephson and R. W. Hales, Phys. Fluids **4**, 373 (1961).
[21] R. G. Fowler and E. B. Turner, Phys. Fluids **4**, 544 (1961).
[22] K. Thom, J. Norwood, and N. Jalufka, Phys. Fluids Suppl. S67 (1964).

assuming $f = 1$ we find values for u_s of 130, 65, 9.3, and 6.5 cm/μsec, respectively, for H_2, He, air, and Ar as compared to an observed speed of 6 cm/μsec. Thus, if the ions carried all the current the drag could be significant for air or Ar but is completely negligible for H_2 or He.

Viscous Drag

We consider next the possibility of drag due to the growth of a viscous boundary layer on the electrodes behind the current sheet. Unfortunately, there has been no theoretical treatment of such a highly cooled magnetohydrodynamic boundary layer, and it is extremely difficult to estimate its thickness due partly to the uncertainty in conditions behind the current sheet and partly to the fact that both the kinetic mean free path λ (cm) $= 10^{15}/n$ (cm^{-3}) and the characteristic ion Larmor radius r_L (cm) $= Au_s$ (cm/μsec) r (cm)$/2I$ (kA) in the range of interest are the same order of magnitude as the annulus spacing (A is the atomic number of the gas). Therefore, our discussion of the viscous boundary layer will necessarily be limited to considerations of a qualitative nature.

We observe first that, if viscous effects are to provide an explanation of the limiting speed, the boundary layer behind the current sheet must grow sufficiently to close the annulus. Otherwise there can be no appreciable flow of current across the annulus behind the leading sheet, and the magnetic pressure will be the same behind the sheet as it is at the driver end. For this to occur within the available test time, the boundary layer would have to grow at a speed of at least 10% of the sheet speed, which seems extremely unlikely in view of the strong cooling that occurs at the walls. On the contrary it is more likely that particles striking the walls will tend to stick and that the region behind the current sheet will be cryogenically pumped.

If the boundary layer did grow sufficiently to close the annulus during the test time, however, we should expect an attenuation of both the flux and sheet speeds since the drag would increase with the length of the closed region. As can be seen in Figs. 5 and 6 no such attenuation was observed and both the flux and sheet speeds were remarkably uniform. We may further note that if viscous effects were important they should be most apparent in the case of small annulus spacing. This is a contradiction of the data in Figs. 3 and 7 which shows that the observed speeds were closer to the calculated speeds for small annulus spacing than for large.

Although a quantitative treatment of the boundary layer problem is to be desired, we believe the qualitative arguments given above are sufficient to rule out any serious possibility that the limiting speed observed can be the result of pure viscous drag.

Drag Due to Ablation

In our opinion the most probable explanation of the limiting speed is that it is due to the inertial drag of material ablated from the walls of the shock tube into the region behind the current sheet. The most likely sources of such material are: (1) the arc spots on the electrodes at the edges of the current sheet and (2) the insulating wall at the driver end of the tube.

The situation encountered in the first case is basically similar to that just discussed, except the boundary layer may contain considerably more material and can be expected to be somewhat thicker. The same arguments apply, however, and it appears improbable that ablation of material by the arc spots can provide an explanation of the observations.

The situation encountered in the second case is more interesting and worth serious consideration. We observe first that under the conditions existing in the interior of the shock tube we must certainly expect material to be ablated from the insulating wall at the driver end of the shock tube. This material will quickly become ionized and, since it is at rest in a strong electric field, a current will flow producing both joule heating and acceleration on the material. Although most of the heat produced is probably convected down the shock tube we may expect that a fraction of it will return to the wall by conduction and produce further ablation. Thus, the ablation process becomes self-sustaining and it is possible to conceive of a situation in which material is continuously generated and accelerated down the shock tube by a steady or quasi-steady current flowing at the driver end. Under these conditions only a part of the driver current supplied to the shock tube would flow in the current sheet and both the sheet and flux speeds would be reduced. It may be noted that the situation is somewhat similar to that in a coaxial arc jet except that the flow rate is controlled by the current and the wall imposes a boundary condition.

An attempt to illustrate the situation graphically has been made in Fig. 11 which shows the process unfolding on a space-time diagram together with assumed profiles for the magnetic field B, electric field E, material velocity u and current density j at a fixed time after the sheet speed has reached a steady

value. The flow has been divided into five regions: (1) a photo-ionized region ahead of the current sheet, (2) a relatively thin region in which the gas swept up by the current sheet is accelerated, (3) a region containing ablated material which grows with time but in which B, E, and u are constant and j is zero, (4) a region of length l in which the ablated material is accelerated by a current at the wall and (5) a thermal boundary layer of thickness δ from which heat is conducted to the back wall to produce ablation.

A full theoretical analysis of the flow based on the model presented above is beyond the scope of the present paper. However, we can obtain some insight into the model by treating the problem in reverse and using the experimental observations in conjuction with the conservation equations to obtain an estimate of the conditions which must exist in the thermal layer. Our analysis will be limited to order of magnitude considerations and we shall neglect all radial gradients. We shall also assume that the thickness of the thermal layer is small compared to the distance in which the flow is accelerated, and that the flow is at least quasi-steady so the partial derivatives with respect to time may be neglected. Under these conditions the equations for conservation of mass, momentum and energy for the thermal layer are

$$m_a n_\delta u_\delta = \dot{m}_a, \tag{11}$$

$$\Delta p + \dot{m}_a u_\delta = j_0 B_0 \delta, \tag{12}$$

$$\dot{m}_a(u_a^2 + u_\delta^2/2) = j_0 E_0 \delta, \tag{13}$$

where m_a is the mean molecular weight of the ablated material, $\dot{m}_a$ is the mass ablation rate, Δp is the pressure rise across the thermal layer, u_a^2 is the energy required to ablate a unit mass of material and the subscripts 0 and δ denotes quantities evaluated at the wall and the edge of the thermal layer, respectively. In obtaining Eq. (13) we have set the term $[uh - (\bar{c}\lambda)\, dh/dz]_\delta$ representing the net enthalpy transport by convection and conduction across the boundary between regions 4 and 5 in Fig. 11 equal to zero. This defines the thickness of the thermal layer

$$\delta = \lambda_\delta / M_\delta \tag{14}$$

where $M = u/\bar{c}$ is the Mach number of the flow and λ is the mean free path for energy transport.

If the density ratio across the current sheet is large then the thickness of the slug of test gas will be small and the final velocity of the ablation products will be approximately equal to the speed of the current sheet. Under these conditions the characteristic

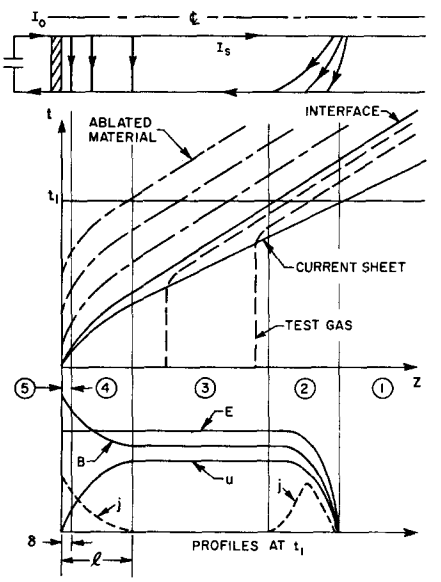

FIG. 11. x–t diagram showing proposed flow model for a magnetic annular shock tube with an ablating wall.

length l in which the ablation products are accelerated may be defined by the equation

$$j_0 B_0 l = \dot{m}_a u_s \tag{15}$$

and the over-all equation for momentum balance is

$$B_0^2/2\mu_0 = n_1 m_1 u_s^2 + \dot{m}_a u_s \tag{16}$$

where n_1 and m_1 are, respectively, the number density and molecular weight of the gas ahead of the leading current sheet.

In addition to the conservation equations, we require an Ohm's law. We anticipate that the gas in the thermal layer will be only slightly ionized and that ion slip will play an important role in determining the conductivity. The appropriate Ohm's law is[23]

$$j = \frac{\sigma}{(1 + \omega_e \tau_e \omega_i \tau_i)} (E + uB) \tag{17}$$

where $\sigma = n_e e^2 \tau_e / m_e$ is the gas conductivity, ω is the cylotron frequency, τ is the collision time and the subscripts e and i refer to electrons and ions, respectively.

To obtain an explicit solution to our problem Eqs. (11) through (17) must be combined with a set of rate equations describing the various chemical and physical processes which together determine the internal state of the ablation products. Since we are not currently in a position to even consider doing this, we propose instead to use these equations to

[23] J. A. Fay, Avco-Everett Research Laboratory Report AMP 83 (1961).

deduce the conditions which must exist in the thermal layer from the experimental observations. To avoid algebraic complications we shall assume, subject to later verification, that

$$\Delta_p \ll \dot{m}_a u_\delta, \tag{18a}$$

$$u_\delta^2/2 \ll u_a^2, \tag{18b}$$

$$1 \ll \omega_e \tau_e \omega_i \tau_i, \tag{18c}$$

$$u_\delta \ll E_0/B_0. \tag{18d}$$

Under these conditions, Eq. (11) to (17) may be combined to give

$$\frac{\delta}{l} = \frac{u_\delta}{u_s} = \left(\frac{u_a}{u_L}\right)\left(\frac{u_a}{u_s}\right) \tag{19}$$

$$\frac{n_\delta}{n_1} = \frac{\lambda_1}{\lambda_\delta} = \left(\frac{m_1}{m_a}\right)\left[\left(\frac{u_1}{u_s}\right)^2 - 1\right]\left(\frac{u_L}{u_a}\right)\left(\frac{u_a}{u_s}\right), \tag{20}$$

$$\frac{\delta}{\lambda_\delta} = \frac{1}{M_\delta} = \left(\frac{u_L}{u_a}\right)\left(\frac{\bar{c}_\delta}{u_a}\right), \tag{21}$$

$$\left(\frac{n_e}{n}\right)_\delta = \left(\frac{Q}{Q_i}\right)\left(\frac{u_a}{u_L}\right)^4\left(\frac{u_a}{\bar{c}_\delta}\right)^2, \tag{22}$$

where u_1 is defined by Eq. (4), E_0/B_0 has been set equal to u_L and Q and Q_i are, respectively, the cross sections for energy and momentum transport.

We may now use the data of Figs. 3 and 7 to evaluate Eqs. (19) through (22). We assume that for lucite which was the material of our insulator $u_a \sim 1$ cm/μsec corresponding to an effective heat of ablation of 4×10^7 J/kg and that the heavy particle temperature of the dissociating ablation products in the thermal layer will be in the vicinity of 10 000°K corresponding to $\bar{c} \sim 0.5$ cm/μsec for particles having a mean weight of 10 atomic units. Then for $u_1 \sim 20$ cm/μsec, $u_L \sim 3$ cm/μsec and $u_s \sim 6$ cm/μsec which are typical values for the velocity limited region, we find from Eqs. (17), (19), and (22)

$$\dot{m}_a/n_1 m_1 u_s \sim 10, \tag{23}$$

$$\delta/l \sim 1/18, \tag{24}$$

$$(n_e/n)_\delta \sim 1/200, \tag{25}$$

where we have assumed $Q/Q_i = 1/10$. Equation (23) shows that for the conditions chosen the mass flux of ablation products is an order of magnitude larger than the mass flux incident on the current sheet while Eqs. (24) and (25) show that the thickness of the thermal layer relative to the acceleration length and the degree of ionization at the edge of the thermal layer are both small as assumed. We see further from Eq. (21) that the Mach number of the flow at the edge of the thermal layer is close to unity as might be expected since this is the condition which determines when a disturbance can propagate toward the back wall.

An estimate of the absolute thickness of the thermal layer for test gas densities in the range 10^{15} to 10^{16} cm^{-3} used in the experiments may be obtained by combining Eqs. (20) and (21). Assuming $Q \sim 10^{-15}$ cm^2 and $(m_1/m_a) \sim 1$ we find $\delta \sim 10^{-2}$ to 10^{-3} cm which is very small compared to typical shock tube dimensions.

We may now check the validity of assumptions (18a) to (18d) made in obtaining these results. It can be seen immediately from Eq. (19) that (18b) and (18d) are both satisfied for the assumed conditions. To determine whether (17c) is satisfied we must evaluate

$$\omega_e \tau_e \omega_i \tau_i = \left(\frac{8\pi r_0}{Q_e Q_i n_e}\right)_\delta \left(\frac{m_1}{m_a}\right)\left(\frac{u_1^2}{\bar{c}\bar{c}_e}\right)_\delta \left(\frac{n_1}{n_\delta}\right) \tag{26}$$

where $r_0 = 2.8 \times 10^{-13}$ cm is the classical electron radius, $\bar{c}_e$ is the electron thermal speed and Q_e is the Coulomb cross section. Inserting the numerical values used above in Eq. (26) gives $\omega_e \tau_e \omega_i \tau_i \sim 10^2$ to $10^3 (T_e/10^5)^{\frac{1}{2}}$ for the density range covered by the experiments. Thus for $T_e \gg 10^{4}$°K, $\omega_e \tau_e \omega_i \tau_i \gg 1$ and assumption (17c) is satisfied.

The final condition which must be met to insure the consistency of our analysis is (17a). To determine when this is the case, we note that heat conduction to the wall must be balanced by ablation so that

$$\dot{m}_a u_a^2 \sim (\bar{c}\lambda)_\delta \left(\frac{\gamma}{\gamma - 1}\right)\frac{\Delta p}{\delta}, \tag{27}$$

where γ is an effective ratio of specific heats for the ablated material. It follows from Eqs. (19), (21), and (27) that for the assumed conditions

$$\Delta p/\dot{m}_a u_\delta \sim \left(\frac{\gamma - 1}{\gamma}\right)\left(\frac{u_L}{u_a}\right)^2 \sim 9\left(\frac{\gamma - 1}{\gamma}\right),$$

which is of order unity for reasonable values of γ. Thus assumption (17a) is not well satisfied and the Δp term in the momentum equation should be retained in a more careful analysis. The order of magnitude of our results should be correct, however.

CONCLUDING REMARKS

In the light of the above analysis it appears likely that ablation of the insulator at the driver end of the shock tube is responsible for limiting the speed of the current sheet in the magnetic annular shock tube employed in these experiments. To obtain a definitive check of this hypothesis it would be desirable to investigate the effect of changing the

material of the insulating walls. Unfortunately, this could not easily be done in conjunction with the present series of experiments because the importance of ablation was not fully appreciated until after the experimental apparatus had been dismantled. It would also be desirable to conduct a more thorough theoretical investigation of the problem to determine whether the steady state situation postulated can actually exist and what factors control the ablation rate of the insulating walls. In this connection it may be noted that the agreement between calculated and measured shock speeds obtained in the experiments of Patrick[1] implies that conditions can exist in magnetic annular shock tubes under which the current detaches from the insulating wall. Since Patrick uses the same material for his insulators as that used in the present experiment, it appears that these conditions must be related either to the presence of bias fields or the methods of pre-ionization and initiation of the discharge. It is also possible that the complicated current and flow patterns[3,6,7] occurring in shock tubes having a large radius ratio have an important effect on the postulated ablation mechanism.

In concluding we should like to point out that the general problem of a current flowing parallel to an insulating wall is encountered in a variety of devices other than coaxial accelerators including magnetohydrodynamic generators, circuit breakers and confined arcs and a detailed analysis of the postulated boundary layer would, therefore, be of considerable practical as well as theoretical interest.

ACKNOWLEDGMENTS

The author would like to express his appreciation to Sumner Freshman who was responsible for operation of the shock tube and collected most of the data presented in this report.

This work has been supported by Air Force Office of Scientific Research, Office of Aerospace Research, United States Air Force under Contract AF49(638)-659.